RSC Advances

PAPER

View Article Online
View Journal | View Issue

Cite this: *RSC Adv.*, 2017, **7**, 50634

Determination of pentachlorophenol by anodic electrochemiluminescence of $Ru(bpy)_3^{2+}$ based on nitrogen-doped graphene quantum dots as co-reactant†

Lijun Luo, Libo Li, Xixi Xu, Dong Liu, Jinyang Li, Kun Wang* and Tianyan You*

Received 15th September 2017
Accepted 10th October 2017

DOI: 10.1039/c7ra10247j

rsc.li/rsc-advances

Sensitive and quantitative analysis of pentachlorophenol (PCP) is especially important in the field of ecology and agriculture. Herein, a highly sensitive and stable $Ru(bpy)_3^{2+}$-based anodic electrochemiluminescence (ECL) system utilizing nitrogen-doped graphene quantum dots (NGQDs) as a novel co-reactant was firstly constructed to detect PCP. In this system, $Ru(bpy)_3^{2+}$ was used as luminophor, while NGQDs were applied as co-reactant in place of the toxic and volatile tripropylamine. The novel co-reactant not only promoted the luminous efficiency of $Ru(bpy)_3^{2+}$, but also improved the stability of the ECL system. In addition, the enhancement mechanism of NGQDs on $Ru(bpy)_3^{2+}$ and quenching mechanism of PCP on $Ru(bpy)_3^{2+}$/NGQDs were investigated in detail. Under the optimum conditions, the as-fabricated sensor for ultrasensitive PCP determination expressed a wider linear range of 1×10^{-15} to 1×10^{-5} g mL^{-1} and a lower detection limit of 2×10^{-17} g mL^{-1} with good stability and repeatability. Furthermore, based on the distinctive advantages of the novel ECL sensor, it was successfully used to detect PCP in tap water and river water, and satisfactory recoveries were obtained.

1. Introduction

Pentachlorophenol (PCP) is usually used as a wood aseptic agent, weedicide, and antifungal agent in industry and agriculture.[1,2] However, PCP possesses serious toxicity and is very harmful to the environment and human health. Therefore, PCP has been listed as priority pollutant and as a persistent organic pollutant by the United States Environmental Protection Agency (US EPA).[3,4] Moreover, the European Union and the US EPA have strictly limited the maximum admissible concentration (0.5 ppb and 1 ppb, respectively) of PCP in drinking water.[5,6] Thus, extensive efforts have been made towards the trace and ultra-trace detection of PCP in the last decade. Various methods, including capillary electrophoresis,[7] gas chromatography (GC),[8] gas chromatography-mass spectrometry (GC-MS),[9] high-performance liquid chromatography (HPLC)[10] and fluorescence detection (FL)[11] have been explored for the measurement of PCP. These detection methods can get good results, but in the actual sample detection analysis, the sensitivity and selectivity still need to be further improved.

In recent years, the development of an electrochemiluminescent (ECL) sensor for the detection of PCP has attracted more and more attention owing to its miniaturization, inexpensive detection instrument, high sensitivity and rapid response. Using Au nanoclusters as luminophor with $S_2O_8^{2-}$ as co-reactant, Luo *et al.*[12] constructed a cathodic ECL sensor to detect PCP with an unprecedented sensitivity. In order to further improve the sensitivity of the developed ECL sensor based on novel ZnO-nanocrystal composites, Jiang *et al.*[13] introduced graphene into the ECL system as a substrate and signal amplification reagent, resulting in ECL intensity enhancement by about 4.3-fold. Currently, with the development of carbon material science, many ECL systems based on carbon nanomaterials, such as graphene,[14] g-C_3N_4,[15] and graphene quantum dots (GQDs)[16] have been widely used for detection. Among them, the ECL of GQDs, especially the heteroatom-doped GQDs, have attracted wide attention owing to their unique features, including good water solubility, low toxicity and better edge effect.[17] For example, Li *et al.*[18] built a novel ECL sensor based on carbon quantum dots with $S_2O_8^{2-}$ as co-reactant to detect PCP, achieving a low limit of detection. Similarly, utilizing nitrogen-doped GQDs (NGQDs) as luminophor, Du *et al.*[19] constructed a cathodic ECL sensor for the detection of PCP. The introduction of N atoms significantly enhanced the stability and reproducibility in comparison with GQDs. However, most of the above-mentioned ECL systems for PCP detection are mainly based on the cathodic ECL system. To the best of our knowledge, the use of anodic ECL system for the detection of PCP is rarely reported.[20]

School of Agricultural Equipment Engineering, Institute of Agricultural Engineering, Jiangsu University, Zhenjiang, Jiangsu 212013, China. E-mail: youty@ujs.edu.cn; Fax: +86-511-88982992; Tel: +86-511-88982992

† Electronic supplementary information (ESI) available. See DOI: 10.1039/c7ra10247j

$Ru(bpy)_3^{2+}$ is a typical anodic ECL luminophor possessing many distinguishing features, such as recyclability, high luminous efficiency, chemical stability and excellent biocompatibility.[21] Therefore, the $Ru(bpy)_3^{2+}$-based anodic ECL system is widely applied in many fields.[22–26] However, tripropylamine (TPA), as the traditional co-reactant of $Ru(bpy)_3^{2+}$, has undesirable volatility and toxicity, as well as low sensitivity at low concentrations. Hence, it is extremely imperative to develop alternative co-reactants to TPA. Recently, it has been reported that carbon quantum dots (CQDs) can be innovatively utilized as co-reactant of $Ru(bpy)_3^{2+}$ to fabricate the anodic ECL system.[27,28] We also carried out some preliminary work on a $Ru(bpy)_3^{2+}$/CQDs ECL system,[29,30] which showed that using carbon dots or related composites as the co-reactant of $Ru(bpy)_3^{2+}$ resulted in good analytical performance for bisphenol A or dopamine detection. Nevertheless, it is well known that the exploration of anodic ECL systems based on $Ru(bpy)_3^{2+}$/GQDs is still in its infancy.

Herein, we utilize nitrogen-doped graphene quantum dots (NGQDs) as the co-reactant of $Ru(bpy)_3^{2+}$ to establish an anodic ECL sensor for PCP detection and to solve the problem of low sensitivity and poor stability. Effects of some experimental conditions on the ECL system were optimized, and the detection of PCP in real samples was analyzed under the optimum conditions. Furthermore, the enhancement mechanism of NGQDs and quenching mechanism of PCP on ECL signals were studied in detail.

2. Experimental

2.1. Reagents and materials

Tris(2,2-bipyridyl)dichlororuthenium(II)hexahydrate ($Ru(bpy)_3Cl_2 \cdot 6H_2O$) was purchased from Sigma-Aldrich. Ammonium citrate tribasic was obtained from Sinopharm Chemical Reagent Co., Ltd. Pentachlorophenol (PCP) and 2,3,5-trichlorobenzene (2,3,5-TCP) were provided by AccuStandard. 2,4-dichlorophenol (2,4-DCP) was purchased from Aladdin, while 2,4-dinitrophenol (2, 4-DNP) was provided by TCI Development Co., Ltd. (Shanghai). NaOH, Na_2HPO_4, NaH_2PO_4, ethanol, methanol, *etc.* were of analytical grade and used as received.

2.2. Apparatus and characterization

Transmission electron micrographs (TEM) were obtained with a TECNAI F20 field-emission TEM at an acceleration voltage of 200 kV. Fourier-transform infrared spectra (FT-IR) of nitrogen-doped graphene quantum dots were recorded on a spectrometer (Nicolet Nexus 470 FTIR). The UV-vis spectra were measured on a UV-2450 spectrophotometer (Shimadzu, Japan). All fluorescence (FL) spectra were acquired using a Hitachi F-4500 FL spectrophotometer (Tokyo, Japan). X-ray photoelectron spectroscopy (XPS) was performed on a Thermo ESCALAB 250 instrument, coupled with Al Kα radiation (VG Scientific, UK). The ECL emission measurements were conducted on a model MPI-EII multifunction chemiluminescence detector (Xi'an Remax Electronic Science & Technology Co. Ltd., Xi'an).

2.3. Preparation of NGQDs

NGQDs were synthesized according to previous literature,[31] with a simple reflux method for preparing NGQDs under atmospheric pressure. Briefly, 2 g ammonium citrate tribasic and 60 mL H_2O were placed into a three-necked flask and heated to 200 °C in an oil bath with a reflux device. Reflux was applied to produce the vapour under high temperature and condense it into liquid in the course of the experiment. A balloon was used at the outlet of the condenser pipe for two main functions: the first was to maintain a relatively sealed environment so that nitrogen can be doped into GQDs; the second was to verify that the experiment can be carried out under atmospheric pressure. Then, in the next 30 minutes, the color of the solution changed from colorless to bright yellow, which indicated that NGQDs were formed. Finally, the pH of the resulting solution was adjusted to 7.0 by the addition of 1 mg mL^{-1} NaOH solution, and the obtained NGQD solution was stored at 4 °C until use.

2.4. ECL and EC behavior of the $Ru(bpy)_3^{2+}$/NGQDs anodic ECL system

The buffer solution was prepared by adjusting Na_2HPO_4 and NaH_2PO_4, and the buffer solution containing $Ru(bpy)_3^{2+}$/NGQDs was used as background solution. The EC and ECL measurements were conducted on the MPI-EII multifunction chemiluminescence detector with a photomultiplier tube (PMT) biased at 800 V and potential scanning from 0.2 to 1.25 V. All experiments were carried out on a conventional three-electrode system, where platinum electrode (Pt, 2 mm) was used as working electrode, Ag/AgCl (saturated KCl) electrode as reference electrode and platinum wire as counter electrode. Moreover, all experiments were conducted at room temperature.

2.5. Detection of PCP and treatment of real sample

The detection of PCP was carried out in the prepared background solution. 1×10^{-3} g mL^{-1} PCP stock solution was prepared by dissolving PCP in methyl alcohol, and other concentrations of PCP were obtained by gradual dilution of the PCP using 30 mM pH 7.5 buffer solution.

The tap water and river water samples were obtained from the tap used in the experiment and Yudai River (Jiangsu University), respectively. The water samples were filtered with a 0.22 μm cellulose membrane, and a certain volume of the solution was added to the background solution for PCP assay.

3. Results and discussion

3.1. Morphological and structural characterization of NGQDs

TEM was employed to characterize the morphology of the as-prepared NGQDs (Fig. 1A). It can be obviously observed that NGQDs are well dispersed from each other and have a relatively narrow size distribution in the range of 1.7–3.1 nm, with the average diameter of 2.5 ± 0.4 nm. HRTEM image of NGQDs (inset of Fig. 1A) reveals that the lattice spacing is 2.10 Å, matching well with the (100) facet of graphitic carbon.[41]

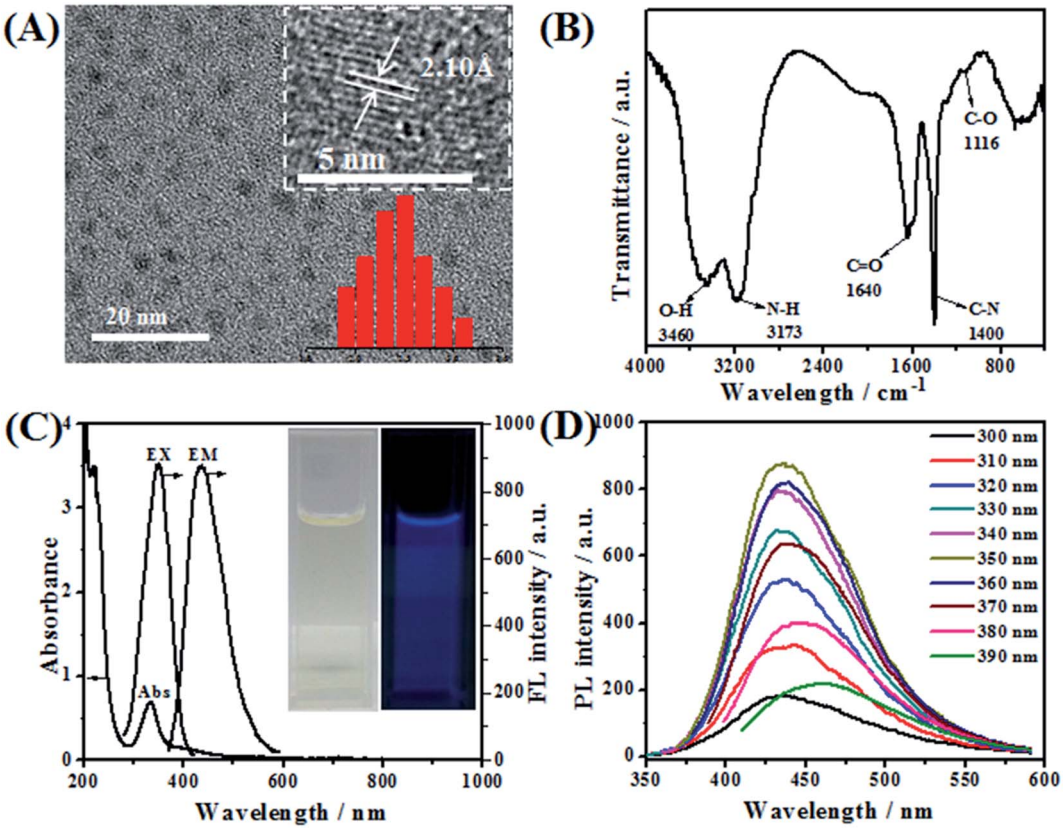

Fig. 1 (A) TEM image of NGQDs. Inset: HRTEM and particle size distribution images of NGQDs, (B) FT-IR spectra, (C) UV-vis absorption and FL spectra, (D) dependence of emission on excitation of the prepared NGQDs. Inset of (C): photographs of NGQDs under white and 365 nm UV light, respectively.

The functional groups on the surface of NGQDs were characterized by FT-IR measurement. As can be seen from Fig. 1B, the broad peaks at 3460 and 3173 cm^{-1} indicate the presence of O–H and N–H bonds, respectively. The band around 1640 cm^{-1} is assigned to the C=O stretching vibrations of the carbonyl and carboxyl groups. The appearance of C–N stretching vibration at 1400 cm^{-1} illustrates the successful doping of N[31] into GQDs. In addition, the absorption band at 1116 cm^{-1} is attributed to the stretching vibration of C–O. These results demonstrate that NGQDs are well prepared, and the nitrogen atoms have been successfully doped into GQDs.

The optical performance of NGQDs was investigated by UV-vis and FL spectroscopy. From the UV-vis spectrum (Fig. 1C), it can be observed that NGQDs exhibit one remarkable peak centered at 334 nm, which is ascribed to the π–π* conjugate structures of aromatic sp^2 domains in the NGQDs. The inset of Fig. 1C shows that the bright yellow aqueous solution of NGQDs can emit bright blue fluorescence under UV light of 365 nm. The maximum excitation and emission wavelength of NGQDs are located at 350 nm and 436 nm, respectively. In order to deeply investigate the optical properties of NGQDs, detailed photoluminescence studies were carried out under different excitation wavelengths. In general, the photoluminescence spectra of most carbon nanoparticles are dependent on the excitation wavelength. In other words, the emission wavelength and peak intensity change obviously with the excitation wavelength, attributed to quantum confinement of emission energy traps on the particle surface.[32] In contrast, as shown in Fig. 1D, the as-prepared NGQDs exhibit photoluminescent properties independent of the excitation wavelength. When the excitation wavelength increases from 300 to 390 nm, the emission peak location changes slightly (Fig. 1D), indicating that the surface state of NGQDs is relatively uniform.[33]

3.2. Anodic ECL behavior and possible mechanism of $Ru(bpy)_3^{2+}$/NGQDs system

The electrochemical and anodic ECL behavior of $Ru(bpy)_3^{2+}$ in the presence of NGQDs and PCP were investigated in detail. First, as can be seen from the cyclic voltammetry (CV) (Fig. 2A, a), $Ru(bpy)_3^{2+}$ shows an obvious oxidation peak and reduction peak current at 1.15 V and 1.03 V, respectively. In contrast, NGQDs (Fig. 2A, b) show no oxidation or reduction peak. However, upon addition of 5 mg mL^{-1} NGQDs to the $Ru(bpy)_3^{2+}$ system (Fig. 2A, c), the oxidation peak current of $Ru(bpy)_3^{2+}$ enhances obviously and the reduction peak current decreases, indicating that NGQDs have a significant catalytic effect on $Ru(bpy)_3^{2+}$.[26] However, further introduction of 50 μg mL^{-1} PCP (Fig. 2A, d) results in the reduction of both oxidation and reduction peak current, demonstrating that PCP has obvious quenching effect on the $Ru(bpy)_3^{2+}$/NGQDs system.

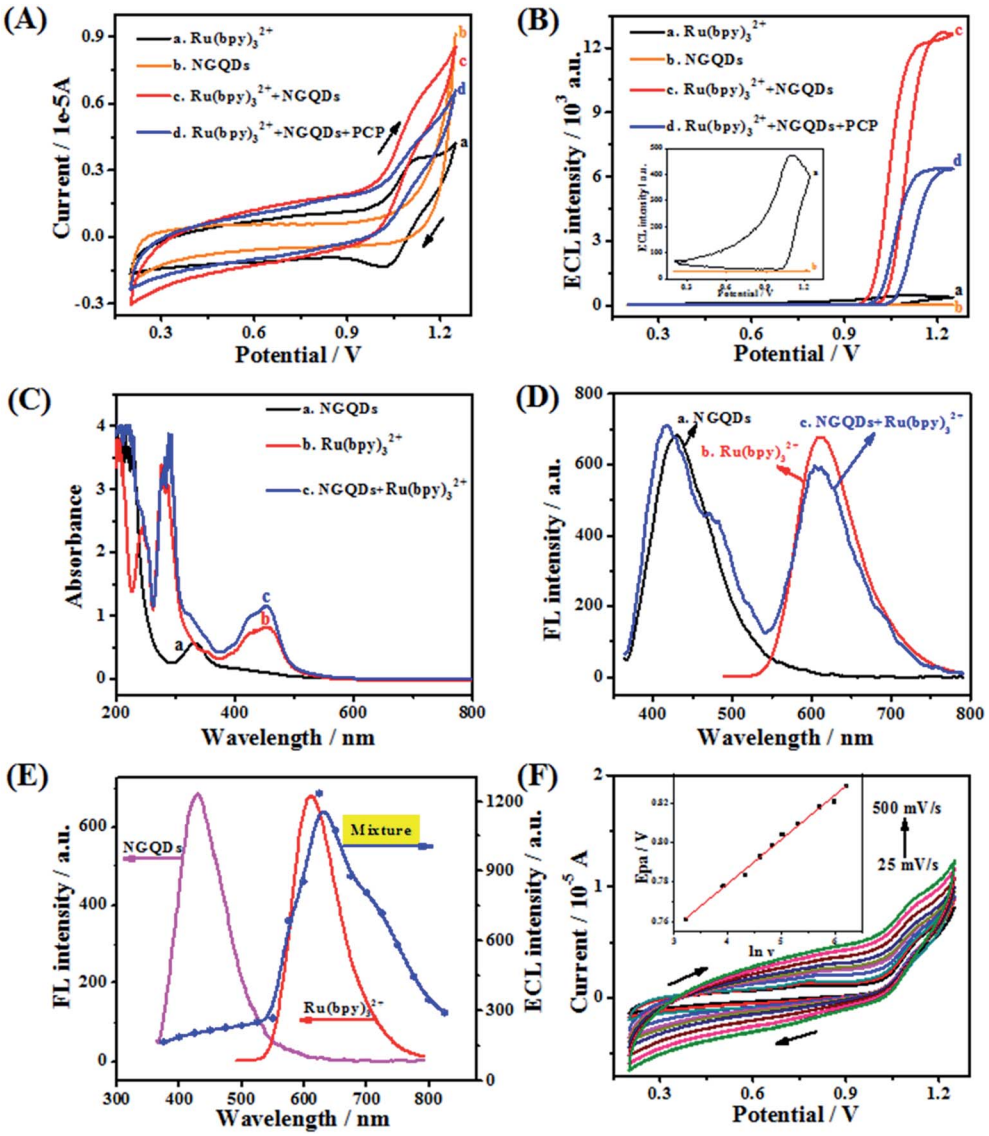

Fig. 2 (A) CVs and (B) corresponding ECL-potential curves of $Ru(bpy)_3^{2+}$ (a), NGQDs (b), $Ru(bpy)_3^{2+}$/NGQDs (c) and $Ru(bpy)_3^{2+}$/NGQDs/PCP (d). Conditions: buffer solution: 30 mM pH 7.5 Na_2HPO_4–NaH_2PO_4; 5 mg mL^{-1} NGQDs; 0.5 mM $Ru(bpy)_3^{2+}$; 50 μg mL^{-1} PCP; scan rate: 100 mV s^{-1}; PMT: 700 V. Inset is the plot of ECL-potential curves of $Ru(bpy)_3^{2+}$ (a) and NGQDs (b). (C) UV-vis absorption spectra and (D) FL spectra of NGQDs (a), $Ru(bpy)_3^{2+}$ (b), and their mixture (c). (E) FL spectra of NGQDs and $Ru(bpy)_3^{2+}$, and ECL spectrum of their mixture. (F) Dependence of peak currents of the $Ru(bpy)_3^{2+}$/NGQDs system on different scan rates in the presence of 5.0×10^{-5} g mL^{-1} PCP. Inset is the plot of E_{pa} *vs.* ln ν. Conditions: buffer solution: 30 mM pH 7.5 Na_2HPO_4–NaH_2PO_4; 5 mg mL^{-1} NGQDs; 0.5 mM $Ru(bpy)_3^{2+}$; scan rate: 100 mV s^{-1}; PMT: 700 V.

Corresponding ECL-potential curves illustrate that the ECL signal (Fig. 2B, a) of $Ru(bpy)_3^{2+}$ is observed at 1.15 V (*ca.* 400 a.u.), while the signal of NGQDs (Fig. 2B, b) is fairly weak. In contrast, upon the addition of NGQDs to the $Ru(bpy)_3^{2+}$ system, the ECL intensity (*ca.* 12 800 a.u.) of $Ru(bpy)_3^{2+}$ is enhanced by about 30-fold (Fig. 2B, c). The obvious improvement of ECL intensity illustrates that NGQDs indeed can be used as a novel co-reactant of $Ru(bpy)_3^{2+}$. However, with the existence of PCP, the ECL signal is significantly quenched by 50% (Fig. 2B, d), which further proves that PCP has quenching effect on the anodic ECL system and that it is feasible to detect PCP using the $Ru(bpy)_3^{2+}$/NGQDs system.

In order to investigate the enhancement mechanism of NGQDs on $Ru(bpy)_3^{2+}$, UV-vis, FL and ECL spectra are measured in detail. Fig. 2C shows the UV-vis absorption spectra of NGQDs, $Ru(bpy)_3^{2+}$ and their mixture. NGQDs display one characteristic band at 334 nm (Fig. 2C, a), while individual $Ru(bpy)_3^{2+}$ (Fig. 2C, b) exhibits two adsorption peaks at 281 and 455 nm, which are ascribed to the π–π* transition and metal-to-ligand charge transfer, respectively. Meanwhile, it can be observed that the NGQDs/$Ru(bpy)_3^{2+}$ mixture has three absorption peaks (Fig. 2C, c) at 334, 283 and 455 nm, corresponding to the adsorption peaks of NGQDs and $Ru(bpy)_3^{2+}$, respectively, indicating that no direct chemical reaction occurs between them. The FL spectra (Fig. 2D) of the mixture also exhibits the approximate emission features of both NGQDs (417 nm) and $Ru(bpy)_3^{2+}$ (610 nm), which illustrates that NGQDs and $Ru(bpy)_3^{2+}$ maintain their original FL characteristics, further confirming the conclusion

that they do not react with each other. Fig. 2E shows that the ECL spectrum of the $Ru(bpy)_3^{2+}$ and NGQD mixture agrees well with the FL spectrum of $Ru(bpy)_3^{2+}$, but is totally different from that of NGQDs. The results clearly prove that the ECL signal is caused by $Ru(bpy)_3^{2+}$ rather than NGQDs, illustrating that $Ru(bpy)_3^{2+}$ is the luminophor rather than NGQDs, which is consistent with the previous report.[34] More importantly, the NGQDs acted as a novel co-reactant to significantly increase the ECL signal.

Based on the above studies and previous reports,[29,34] we can speculate that the role of NGQDs is similar to that of TPA as co-reactant, which could promote the luminous efficiency of $Ru(bpy)_3^{2+}$. The specific mechanism involved in the presence of NGQDs is described as follows (Scheme 1): first, $Ru(bpy)_3^{2+}$ is oxidized to $Ru(bpy)_3^{3+}$ on the surface of the working electrode; then, $Ru(bpy)_3^{3+}$ reacts with the NGQD intermediate to form an excited $Ru(bpy)_3^{2+}$*. Finally, the return of $Ru(bpy)_3^{2+}$* to its ground state is accompanied by the emission of light at 620 nm.

Cyclic voltammetry was carried out to understand the possible quenching mechanism of PCP on the novel anodic ECL system. Fig. 2F shows that PCP exhibits irreversible electrochemical oxidation at about 0.78 V (*vs.* Ag/AgCl) under the scan rate of 100 mV s^{-1}. The oxidation potential of PCP is more negative than that of $Ru(bpy)_3^{2+/3+}$ (1.15 V). Therefore, it can be deduced that the oxidation products of PCP may play an important role in the quenching process. To examine this, the oxidation process of PCP was studied by changing the scan rate from 25 to 500 mV s^{-1}. It can be seen (Fig. 2F) that with the increase of the scan rate, the oxidation peak potential of PCP gradually shows a positive shift. The inset of Fig. 2F expresses the relationship of peak potential (E_{pa}) and ln ν with the linear regression equation: E_{pa} (V) = 0.6894 + 0.02245 ln ν (V s^{-1}) (R^2 = 0.993). According to Laviron's theory,[35] the E_{pa} can be described by the following equation,

$$E_{pa} = E^0 - \frac{RT}{(1-\alpha)nF} \ln \frac{RTk_s}{(1-\alpha)nF} + \frac{RT}{(1-\alpha)nF} \ln \nu$$

where α, n, and k are the electron transfer coefficient, electron transfer number and standard rate coefficient, respectively. According to the formula, $(1-\alpha)n$ is calculated to be 1.1438. In general, for a completely irreversible electrode process, α is assumed to be 0.5.[36] Therefore, the number of electron transfers (n) can be calculated to be about 2.3, which proves that PCP lost two electrons to form tetra-chloro-benzoquinone (TCQ) (inset of Scheme 1). TCQ belongs to the benzoquinone species, which is well known to be capable of quenching the anodic ECL of $Ru(bpy)_3^{2+}$* *via* energy transfer.[37] Therefore, the quenching mechanism of PCP on the $Ru(bpy)_3^{2+}$/NGQDs ECL system should be related to the electron transfer between the $Ru(bpy)_3^{2+}$* and TCQ. When PCP and the $Ru(bpy)_3^{2+}$/NGQDs system coexist, the electrons transfer from $Ru(bpy)_3^{2+}$* to TCQ, thus reducing the ECL signal of $Ru(bpy)_3^{2+}$/NGQDs (Scheme 1). The quenching mechanism is quite different from previous works on PCP detection based on the cathodic ECL system,[38] where PCP absorbed on the CQD surface is oxidized by C^{*+}, resulting in a decreased ECL intensity. In the cathodic ECL system, electron transfer occurred between the excited C^{*+} and PCP, while TCQ was an oxidation product. However, in the present work, TCQ played an important role in quenching the ECL intensity of the $Ru(bpy)_3^{2+}$/NGQDs system. Therefore, based on the efficient quenching effect, we firstly developed a sensitive and selective anodic ECL sensing platform for PCP assay.

3.3. Optimization of conditions for the $Ru(bpy)_3^{2+}$/NGQDs system in PCP detection

In order to obtain the best analytical performance, a series of experimental conditions were optimized.

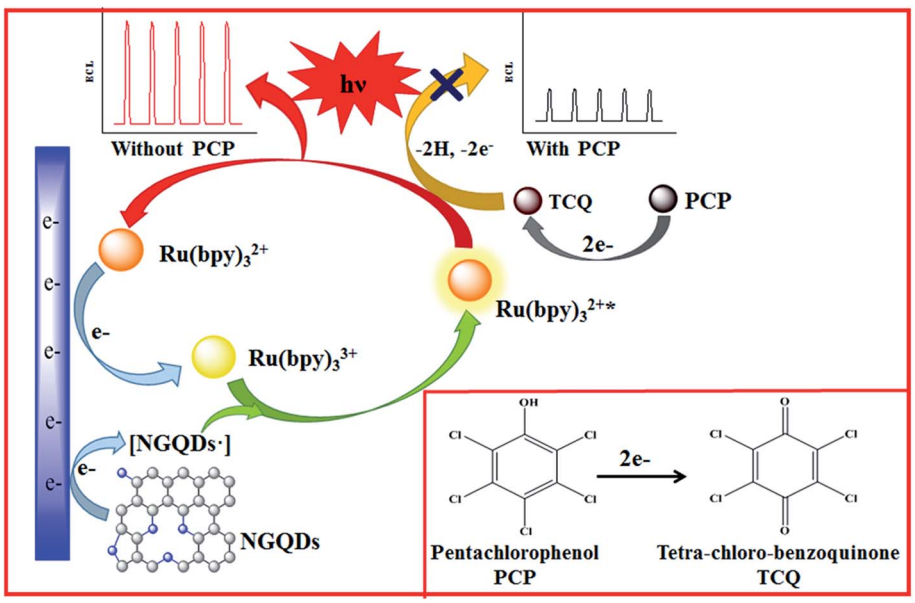

Scheme 1 The possible enhancement mechanism by NGQDs and quenching mechanism by PCP of the ECL system.

The concentration of NGQDs is a very key factor that affects ECL intensity (I_{ECL}). Thus, the influence of NGQDs on I_{ECL} was investigated in the range of 1–10 mg mL^{-1}. As indicated in Fig. 3A, I_{ECL} increases with increasing NGQD concentration from 1 mg mL^{-1} to 5 mg mL^{-1}, while it begins to decrease when the concentration exceeds 5 mg mL^{-1}. As described earlier, NGQDs could promote the luminous efficiency of $Ru(bpy)_3^{2+}$; thus, I_{ECL} increases with higher NGQD amounts. However, the inner filter effect from a high concentration of NGQDs could cause a secondary reaction,[27] which could decrease the I_{ECL}. Therefore, the optimum NGQD concentration is chosen as 5 mg mL^{-1}.

Concentration of $Ru(bpy)_3^{2+}$ is another important factor that influences ECL intensity. Fig. 3B shows that the ECL signal increases correspondingly when the concentration of $Ru(bpy)_3^{2+}$ increases from 0.1 mM to 0.5 mM; then, I_{ECL} begins to drop off thereafter. This is due to the increase of $Ru(bpy)_3^{2+}$, which results in more luminophors dispersed in the solution, resulting in a higher ECL response. When the concentration is too high, the ECL emission may be absorbed or scattered.[39] Thus, 0.5 mM $Ru(bpy)_3^{2+}$ is selected for sensor preparation.

Since the ECL of the $Ru(bpy)_3^{2+}$/NGQDs system is a pH-dependent reaction, the effect of buffer solution pH on the ECL response was investigated (Fig. 3C). The I_{ECL} increases with pH value in the range of 5.0–7.5, while it begins to gradually decrease at higher pH value. The increase of I_{ECL} should be attributed to the comprehensive effect of pH value on $Ru(bpy)_3^{2+}$ consumption[40] and NGQD deprotonation. However, extremely high pH value would cause decomposition of some species, which further leads to decreased ECL signal and an unstable system. Consequently, the pH value is designated as 7.5 in subsequent experiments.

In addition, the concentration of buffer solution also plays a significant role in constructing the $Ru(bpy)_3^{2+}$/NGQDs ECL system (Fig. 3D). The maximum ECL signal can be obtained at a buffer concentration of 30 mM. This could be attributed to the fact that with increasing concentration, the buffering effect becomes better. However, too high ionic strength of the solution caused by higher buffer concentration will result in reduced ECL signal. Hence, 30 mM pH 7.5 buffer solution is used throughout the experiments.

3.4. Analytical performance for PCP detection

Since PCP can quench the anodic ECL signal, we used the $Ru(bpy)_3^{2+}$/NGQDs system to analyze PCP under the optimal conditions. The quenched ECL intensities are defined as ΔI_{ECL}, and $\Delta I_{ECL} = I_0 - I$, where I_0 and I represent the ECL intensities of the $Ru(bpy)_3^{2+}$/NGQDs system in the absence and presence of PCP, respectively. ΔI_{ECL} increases linearly with the logarithmic PCP concentration from 1×10^{-15} to 1×10^{-5} g mL^{-1} (Fig. 4A

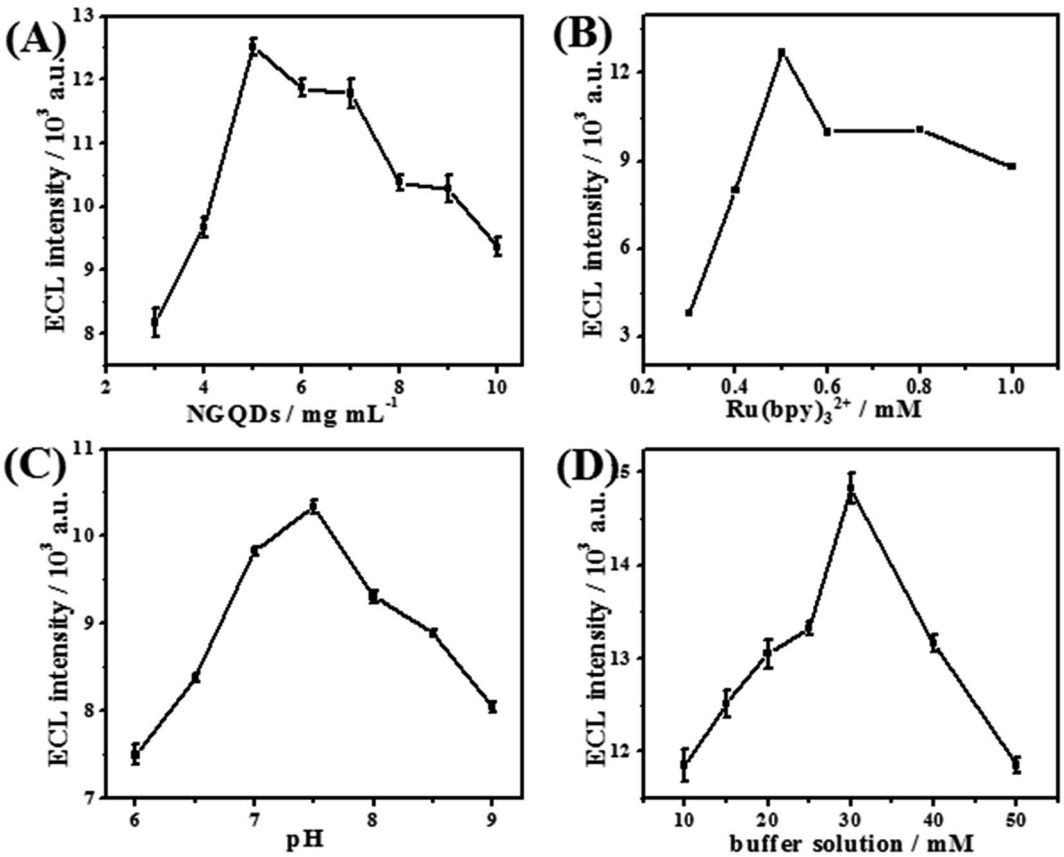

Fig. 3 Optimization of experimental parameters: (A) NGQD concentration, (B) $Ru(bpy)_3^{2+}$ concentration, (C) pH value, and (D) concentration of buffer solution.

and B) with a correlation coefficient of 0.998, and the calibration curve is $\Delta I_{ECL} = 8389.88 + 527.7 \log C_{PCP}$. The limit of detection (LOD) for PCP analysis using the developed sensor was calculated (using 3σ method) to be 2×10^{-17} g mL^{-1}. Compared with previous ECL sensors for PCP detection, it can be clearly seen from Table 1 that the as-prepared $Ru(bpy)_3^{2+}$/NGQDs anodic ECL sensor exhibits a wider linear range, which spans ten orders of magnitude. We also obtain the lowest detection limit for PCP in comparison with other sensors, indicating the highest sensitivity of the proposed sensor.

To investigate the selectivity of the established ECL sensor, 2,3,5-trichlorophenol (TCP), 2,4-dichlorophenol (DCP) and 2,4-dinitrophenol (DNP) were used as interfering substance to evaluate the specificity of the proposed sensor (Fig. 4C). The results indicate that the addition of 0.5 μg mL^{-1} (5 times of PCP) DCP, DNP and TCP lead to only 2.7%, 3.3% and −4.5% decreases in ECL intensity of the $Ru(bpy)_3^{2+}$/NGQDs system, respectively. The addition of 0.1 μg mL^{-1} PCP results in a 38.3% decrease in ECL intensity, indicating that the sensor has good selectivity for PCP detection. Moreover, there are some other interfering ions in real water samples, such as metal ions (Na^+, K^+, Ca^{2+}, Mg^{2+}) and inorganic ions (Cl^-, NO_3^-, SO_4^{2-}). Thus, the effects of these interferences were also examined, and the results show these ions (*c.a.* 10 times of PCP) have no interference on the ECL system. All of these results prove that the fabricated sensor has a high selectivity for PCP detection.

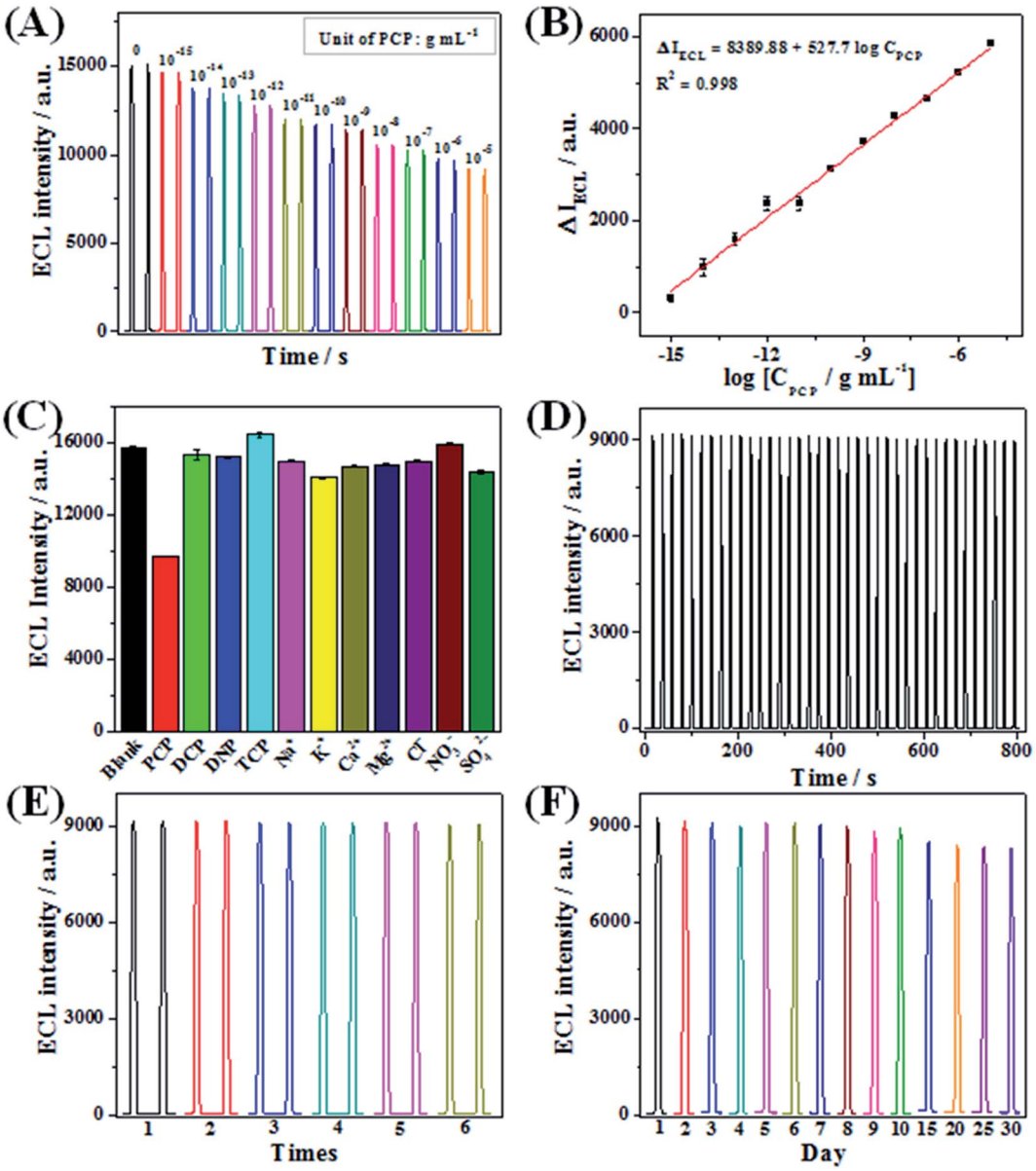

Fig. 4 (A) The ECL intensity of the $Ru(bpy)_3^{2+}$/NGQDs ECL system at different concentrations of PCP. (B) Linear calibration curve for PCP detection (error bars denote S.D.). (C) The selectivity of the sensor with different interferences. (D) The stability of the proposed sensor in the presence of PCP under consecutive cyclic scan of 40 cycles. (E and F) Repeatability of PCP detection by 6 parallel measurements and continuous measurements for one month.

Table 1 Performance comparison of the proposed sensor with other methods

Methods	ECL	Linear range (g mL^{-1})	LOD (g mL^{-1})	Reference
Au NCs-GR/$S_2O_8^{2-}$	Cathodic	2.66×10^{-15}–2.66×10^{-11}	2.66×10^{-15}	12
ZnO/N-GR/GCE/$S_2O_8^{2-}$	Cathodic	1.33×10^{-13}–1.63×10^{-8}	4.27×10^{-14}	13
GQDs-CdS NCs/GCE/H_2O_2	Cathodic	1×10^{-11}–5×10^{-7}	3×10^{-12}	19
Luminol/GQDs-Cu_2O	Anodic	2×10^{-11}–3×10^{-6}	6.6×10^{-12}	20
$Ru(bpy)_3^{2+}$/NGQDs	**Anodic**	**1×10^{-15}–1×10^{-5}**	**2×10^{-17}**	**This work**

The stability and repeatability of the anodic ECL sensor were evaluated systematically. Firstly, the operational stability of the sensor was investigated by consecutively scanning for 40 cycles and recording the ECL signals of the $Ru(bpy)_3^{2+}$/NGQDs system in the presence of PCP. As seen from Fig. 4D, the ECL response exhibits a desirable consistency with a relative standard deviation (RSD) of only 1.1%, suggesting the high stability of the ECL sensor for PCP detection, which is attributed to the introduction of NGQDs. Secondly, operational and long-term storage repeatability of the sensor were also evaluated. On the one hand, operational repeatability was examined using six different working electrodes. The RSD of six parallel experiments is calculated to be 0.4% (Fig. 4E). On the other hand, the as-prepared sensor is stored at room temperature, and the ECL response of the sensor was continuously recorded every day for one month, with a RSD of 3.5% (Fig. 4F). These results fully demonstrate the ideal repeatability of the $Ru(bpy)_3^{2+}$/NGQDs anodic system.

3.5. Analytical application of the sensor in real samples

In order to verify the practicality of the proposed ECL sensor, recovery experiments were conducted by adding different amounts of PCP into tap water and river water samples. The results are presented in Table S1,† where it can be found that satisfactory recoveries of 96.2–102.7% with RSD of 1.04–5.39% are obtained. These results indicate that the developed method can be used for the analysis of PCP in real samples.

4. Conclusion

In summary, a novel ultrasensitive anodic ECL sensor based on $Ru(bpy)_3^{2+}$/NGQDs system was firstly developed for PCP detection. Primarily, the introduction of NGQDs as a co-reactant of $Ru(bpy)_3^{2+}$ not only effectively enhanced the ECL intensity of $Ru(bpy)_3^{2+}$, but also provided excellent stability for the system. Investigation results indicated that PCP had a good quenching effect on the $Ru(bpy)_3^{2+}$/NGQDs anodic ECL owing to the electron transfer between TCQ and $Ru(bpy)_3^{2+}$*. On this basis, an anodic ECL sensor for PCP analysis was constructed. Under the optimum conditions, sensitive analysis of PCP was achieved with a wide detection range, low detection limit, good selectivity and repeatability. Finally, the developed sensor was successfully applied to analysis of PCP in real water samples. The novel $Ru(bpy)_3^{2+}$/NGQDs anodic ECL sensor provides a new perspective to detect phenolic pesticide residue in real samples.

Conflicts of interest

There are no conflicts to declare.

Acknowledgements

This project was supported by the National Natural Science Foundation of China (No. 21475124 and 21675065), the Priority Academic Program Development (PAPD) of Jiangsu Higher Education Institutions (2014-37), the Natural Science Foundation of Jiangsu Province (No. BK20160490) and National key R & D projects "Research on testing method of machine operating state parameters" (No. 2016YFD0700104-1).

References

1 Z. Lin, Z. Zhen, Z. H. Wu, J. W. Yang, L. Y. Zhong, H. Q. Hua, C. L. Luo, J. Bai, Y. T. Li and D. Y. Zhang, *J. Hazard. Mater.*, 2016, **301**, 35–45.
2 M. Wu, L. Wang, G. Xu, N. Liu, L. Tang, J. Zheng, T. Bu and B. Lei, *Environ. Monit. Assess.*, 2013, **185**, 3149–3161.
3 Y. Dudal, A. R. Jacobson, R. Samson and L. Deschenes, *Water Res.*, 2004, **38**, 3147–3154.
4 W. W. Zheng, H. Yu, X. Wang and W. D. Qu, *Environ. Int.*, 2012, **42**, 105–116.
5 H. Xu, X. L. Zhang and J. H. Zhan, *J. Nanosci. Nanotechnol.*, 2010, **10**, 7654.
6 Q. Kang, L. X. Yang, Y. F. Chen, S. L. Luo, L. F. Wen, Q. Y. Cai and S. Z. Yao, *Anal. Chem.*, 2010, **82**, 9749–9754.
7 Y. R. Wang and H. W. Chen, *J. Chromatogr. A*, 2005, **1080**, 192–198.
8 T. Czech, N. B. Bonilla, F. Gambus, R. R González, J. Marín-Sáez, J. L. Vidal and A. G. Frenich, *Sci. Total Environ.*, 2016, **s557–558**, 681–687.
9 C. Mardones, J. Palma, C. Sepulveda, A. Berg and D. V. Baer, *J. Sep. Sci.*, 2003, **26**, 923–926.
10 D. M. Han, G. Z. Fang and X. P. Yan, *J. Chromatogr. A*, 2005, **1100**, 131–136.
11 W. J. Dong, J. P. Song, C. Dong and M. F. Choi, *Chin. Chem. Lett.*, 2010, **21**, 346–348.
12 S. L. Luo, H. Xiao, S. L. Yang, C. B. Liu, J. S. Liang and Y. H. Tang, *Sens. Actuators, B*, 2014, **194**, 325–331.
13 D. Jiang, X. J. Du, Q. Liu, L. Zhou, J. Qian and K. Wang, *ACS Appl. Mater. Interfaces*, 2015, **7**, 3093–3100.
14 X. J. Du, D. Jiang, L. Liu, L. Zhou, J. Qian, H. P. Mao and K. Wang, *Talanta*, 2015, **132**, 146–149.

15 H. F. Xu, S. J. Liang, X. Z. Zhu, X. Q. Wu, Y. Q. Dong, H. S. Wu, W. X. Zhang and Y. W. Chi, *Biosens. Bioelectron.*, 2017, **92**, 695–701.
16 Y. Q. Dong, H. Wu, P. X. Shang, X. T. Zeng and Y. W. Chi, *Nanoscale*, 2015, **7**, 16366–16371.
17 J. H. Shen, Y. H. Zhu, X. L. Yang and C. Z. Li, *Chem. Commun.*, 2012, **48**, 3686–3699.
18 J. Z. Li, N. Y. Wang, T. T. Tran, C. A. Huang, L. Chen, L. J. Yuan, L. P. Zhou, R. Shen and Q. Y. Cai, *Analyst*, 2013, **138**, 2038–2043.
19 X. J. Du, D. Jiang, L. Liu, G. B. Zhu, H. P. Mao and K. Wang, *Analyst*, 2015, **140**, 1253–1259.
20 Y. T. Yan, Q. Liu, X. Y. Dong, N. Hao, S. B. Chen, T. Y. You, H. P. Mao and K. Wang, *Microchim. Acta*, 2016, **183**, 1591–1599.
21 C. Y. Xiong, H. J. Wang, Y. L. Yuan, Y. Q. Chai and R. Yuan, *Talanta*, 2015, **131**, 192–197.
22 Q. M. Feng, Y. Z. Shen, M. X. Li, Z. L. Zhang, W. Zhao, J. J. Xu and H. Y. Chen, *Anal. Chem.*, 2015, **88**, 937–944.
23 X. Lv, Y. Li, T. Yan, X. Pang, W. Cao, B. Du, D. Wu and Q. Wei, *Biosens. Bioelectron.*, 2015, **70**, 28–33.
24 Y. Z. Wang, W. Zhao, P. P. Dai, H. J. Lu, J. J. Xu, J. Pan and H. Y. Chen, *Biosens. Bioelectron.*, 2016, **86**, 683–689.
25 X. J. Li, S. Q. Yu, T. Yan, Y. Zhang, B. Du, D. Wu and Q. Wei, *Biosens. Bioelectron.*, 2017, **89**, 1020–1025.
26 W. Zhang, S. Y. Zhu, R. Luque, S. Han, L. Z. Hu and G. B. Xu, *Chem. Soc. Rev.*, 2016, **45**, 715–752.
27 Z. Xu, J. Yu and G. Liu, *Sens. Actuators, B*, 2013, **181**, 209–214.
28 Y. Xu, J. Liu, C. Gao and E. Wang, *Electrochem. Commun.*, 2014, **48**, 151–154.
29 L. B. Li, B. Yu, X. P. Zhang and T. Y. You, *Anal. Chim. Acta*, 2015, **895**, 104–111.
30 L. B. Li, D. Liu, M. P. Mao and T. Y. You, *Biosens. Bioelectron.*, 2017, **89**, 489–495.
31 Y. Y. Yin, Q. Liu, D. Jiang, X. J. Du, J. Qian, H. P. Mao and K. Wang, *Carbon*, 2016, **96**, 1157–1165.
32 Y. P. Sun, B. Zhou, Y. Lin, W. Wang, S. Fernando, P. Pathak, J. Meziani, B. Harruff, X. Wang, H. F. Wang, P. J. Luo, H. Yang, M. Kose, B. Chen, L. M. Veca and S. Y. Xie, *J. Am. Chem. Soc.*, 2006, **128**, 7756–7757.
33 S. N. Baker and G. A. Baker, *Angew. Chem., Int. Ed.*, 2010, **49**, 6726–6744.
34 Y. M. Long, L. Bao, J. Y. Zhao, Z. L. Zhang and D. W. Pang, *Anal. Chem.*, 2014, **86**, 7224–7228.
35 E. Laviron, *J. Electroanal. Chem. Interfacial Electrochem.*, 1979, **101**, 19–28.
36 S. Feng, R. Yang, X. Ding, J. Li, C. Guo and L. Qu, *Ionics*, 2015, **21**, 3257–3266.
37 J. McCall, C. Alexander and M. M. Richter, *Anal. Chem.*, 1999, **71**, 2523–2527.
38 S. L. Yang, J. S. Liang, S. L. Luo, C. B. Liu and Y. H. Tang, *Anal. Chem.*, 2013, **85**, 7720–7725.
39 L. X. Zhang and S. J. Dong, *Anal. Chem.*, 2006, **78**, 5119–5123.
40 Y. Huang, W. Pan, M. Guo and S. Yao, *J. Chromatogr. A*, 2007, **1154**, 373–378.
41 S. N. Qu, X. Y. Liu, X. Y. Guo, M. H. Chu, L. G. Zhang and D. Z. Shen, *Adv. Funct. Mater.*, 2013, **24**, 2689–2695.